Influence of Dresselhaus spin-orbit interaction on the domain wall magnetoresistance of diluted magnetic semiconductor thin films

V. Fallahi and M. Ghanaatshoar[*]

Laser and Plasma Research Institute, Shahid Beheshti University, G.C., Evin 1983963113, Tehran, Iran
(Received 28 December 2009; revised manuscript received 1 June 2010; published 22 July 2010)

Domain wall magnetoresistance (MR) of an impure magnetic semiconductor layer is studied theoretically within the semiclassical approach. The effect of the Dresselhaus spin-orbit interaction is taken into account and it is shown that this interaction can enhance the domain wall MR. In the absence of Dresselhaus interaction, the domain wall MR decreases monotonously with the domain wall width but presence of the Dresselhaus coupling prevents this reduction for a range of the domain wall thicknesses. It is also revealed that the Dresselhaus spin-orbit interaction is more effective than the Rashba term in producing domain wall resistance in a typical magnetic semiconductor.

I. INTRODUCTION

Spintronics is an emerging class of electronics that utilizes electron's spin for significantly enhanced or fundamentally new device functionality. The devices based on giant magnetoresistance (GMR) and tunneling magnetoresistance effects are the most prominent examples of spintronic devices that have revolutionized the magnetic sensing and recording industries.[1–3] Nearly all devices made so far in spintronics have been based on metallic heterostructures.[4] Newly, semiconductor spintronics has attracted great deal of attention.[5,6] Indeed, the ferromagnetism found in diluted magnetic semiconductors has opened up a completely new road to combine magnetism with charge transport in well-known semiconductor device structures. It is anticipated that the coupled ferromagnetism and electronic transport would make the effect of magnetism significantly stronger than the corresponding phenomena observed in metals. For example, very large MR has been reported in lateral ferromagnetic (Ga,Mn)As wires with nanoconstrictions.[7]

Various spin-dependent scattering mechanisms such as bulk and interface scattering are responsible for GMR effect. The bulk scattering originates from local defects, lattice imperfections, and foreign atoms residing inside the bulk of the constituting layers. The contribution of the interface scattering arises from differences in band structure of adjacent layers at the interfaces. Besides, it is well known that the nanosize domain walls in magnetic systems cause spin-flip scattering via coupling of two spin states and introduce resistance to the flow of currents. For a thick domain wall, where the magnetization changes in a large scale, depending on the energy of carriers, the polarization axis of the carriers may follow the local magnetic moments adiabatically without any relaxation.[8] But in sharp domain walls, spin mistracking for the carriers passing through local magnetic moments causes spin relaxation and leads to a supplementary resistance. Researchers have recently made numerous efforts to realize the resistance of magnetic domain walls. The first attempts of measuring the MR effect resulting from the presence of the domain wall in a single magnetic film were undertaken by Gregg *et al.*[9] Afterward, in the diffusive regime proposed by Levy and Zhang, the positive and relatively

small MR in the bulk ferromagnets was demonstrated.[10] Then, large domain wall MR in magnetic nanostructures with a sharp domain wall was exhibited in the theoretical[11] and experimental[12] analysis on Co nanowires. Alternatively, both positive[13,14] and negative[15,16] contributions of domain walls to the MR have been observed in ferromagnetic semiconductors.

In addition to the above-mentioned mechanisms, the D'yakonov-Perel' process resulting from the lack of inversion symmetry, leads to spin-flip scattering in both metals and semiconductors. This mechanism typically dominates the spin dynamics in III-V semiconductors.[17] The spin polarization of the carriers is scattered during transport because of D'yakonov-Perel' relaxation caused by both the Dresselhaus (due to the bulk inversion asymmetry) and the Rashba (arising out of the presence of structure inversion asymmetry) spin-orbit interactions. We envisage that in low dimensional semiconducting systems the domain wall MR is considerably affected in the presence of the spin-orbit couplings. Through band-structure calculations for zinc-blende magnetic semiconductors, it has been shown that the spin-orbit interaction can lead to a nonzero domain wall resistance even in the adiabatic limit.[18,19] Recently, the effect of the Rashba spin-orbit interaction on the domain wall MR has been calculated by Dugaev *et al.*[20] They demonstrated that the Rashba interaction may result in an increase in the MR of a semiconducting magnetic wire with a domain wall of width d. Such calculations were carried out for the case of a sharp domain wall. This case corresponds to the limit of $k_{F\uparrow(\downarrow)}d \ll 1$, where $k_{F\uparrow(\downarrow)}$ is the magnitude of Fermi vector for the majority (minority) spins. The effect of the Rashba interaction on the MR of a smooth domain wall in ferromagnetic metals has been studied, too. It has been shown that the spin-flip scattering and consequently the resistivity due to the domain wall increases monotonically as the Rashba interaction strength increases.[21,22]

In the present paper, we investigate the effect of Dresselhaus spin-orbit interaction on domain wall resistance in heavily Mn-doped GaAs, a *p*-type ferromagnetic semiconductor. We examine the spin-dependent transport through the domain wall for current-in-wall (CIW) and current-perpendicular-to-wall (CPW) geometries. We also take the
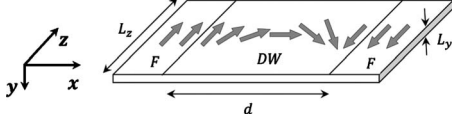
FIG. 1. A Néel-type domain wall with dimensions of $d \times L_y \times L_z$.

Rashba spin-orbit interaction into account to compare its influence on the domain wall MR with that of Dresselhaus spin-orbit term. In this order, we introduce the Hamiltonian which includes the Rashba and the Dresselhaus terms and determine the scattering matrices. We consider a two-dimensional electron-gas (2DEG) system which includes a linear magnetic domain wall between two ferromagnetic regions in opposite directions. The theory is based on the semi-classical Boltzmann equation with the relaxation-time approximation in the elastic regime.

II. THEORETICAL CONSIDERATIONS

We consider a 2DEG containing a 180° Néel-type domain wall of width d in p-type ferromagnetic semiconductor films, in which according to Fig. 1, the magnetic moments rotate in such a manner that a constant angle is maintained between them. Therefore, the functionality of moment's rotation angle can be expressed as $\theta(x) = \pi x / d$.

The Hamiltonian of the system in the presence of the Dresselhaus and the Rashba spin-orbit couplings can be written as

$$H = H_0 + H_{ex} + H_{im} + H_R + H_D, \tag{1}$$

where H_0 contains periodic potential and kinetic energy, H_{ex} is the exchange interaction between the holes and the localized moments, H_{im} represents the interaction of the localized magnetic impurities with the holes, and H_R and H_D include the Rashba and the Dresselhaus spin-orbit interactions, respectively. The three first terms of the Hamiltonian can be expressed as follows:

$$H_0 = \frac{\hbar^2}{2m} \left(\frac{\partial^2}{\partial x^2} + \frac{\partial^2}{\partial z^2} \right) + V(x,z), \tag{2}$$

where $V(x,z)$ is the lattice periodic potential,

$$H_{ex} = -\Delta \hat{\sigma} \cdot \hat{M}(x,z) \tag{3}$$

in which Δ is the spin splitting energy, $\hat{\sigma}$ denotes the spin operators in terms of the Pauli spin matrices and $\hat{M}$ is the unit vector along the direction of local magnetization,

$$H_{im} = \sum_j \left[v_{im} - \Delta_{im} \hat{\sigma} \cdot \hat{M}(x,z) \right] \delta(x - x_j) \delta(z - z_j), \tag{4}$$

where the summation is over all impurities, Δ_{im} stands for the exchange splitting constant between the holes and localized impurities and v_{im} is on-site electrical potential of the localized impurities. The spin-orbit interactions can be written as

$$H_R = i \gamma_R \left(\hat{\sigma}_x \frac{\partial}{\partial z} - \hat{\sigma}_z \frac{\partial}{\partial x} \right) \tag{5}$$

and

$$H_D = -i \gamma_D \left[\left(\frac{\pi}{L_y} \right)^2 \frac{\partial}{\partial x} + \frac{\partial}{\partial x} \frac{\partial^2}{\partial z^2} \right] \hat{\sigma}_x$$
$$+ i \gamma_D \left[\left(\frac{\pi}{L_y} \right)^2 \frac{\partial}{\partial z} + \frac{\partial}{\partial z} \frac{\partial^2}{\partial x^2} \right] \hat{\sigma}_z \tag{6}$$

in which γ_R and γ_D are the Rashba and Dresselhaus interactions strengths, respectively.

The eigenstates of $H_0 + H_{ex}$ for the two-dimensional system are as follows:

$$|\Psi_{\boldsymbol{k}}^\uparrow\rangle = \alpha(k_x) \frac{e^{i(k_x x + k_z z)}}{\sqrt{L_x L_y}} R_{\theta(x)} \begin{pmatrix} 1 \\ i\zeta k_x \end{pmatrix}, \tag{7a}$$

$$|\Psi_{\boldsymbol{k}}^\downarrow\rangle = \alpha(k_x) \frac{e^{i(k_x x + k_z z)}}{\sqrt{L_x L_y}} R_{\theta(x)} \begin{pmatrix} i\zeta k_x \\ 1 \end{pmatrix}, \tag{7b}$$

where $\zeta = \frac{\pi \hbar^2}{4m^* d\Delta}$, $\alpha(k_x) = (1 + \zeta^2 k_x^2)^{-1/2}$ is the normalization coefficient and $R_\theta = \exp[-i\frac{\theta(x)}{2}\sigma_y]$ is the rotation operator for spin of holes. This operator transforms the domain wall into a homogeneous system for passing carriers.[10,23–25] The eigenstates of Eq. (7) are not pure spin states and correspond to energy eigenvalues $\epsilon_{k,\sigma} = \frac{\hbar^2 k^2}{2m^*} - \sigma\Delta$ ($\sigma = +1, -1$ for up- and down-spin bands, respectively). The influence of the periodic potential is included via an effective mass denoted by m^*.

We consider the Boltzmann transport equation to develop the domain wall resistance. For homogeneous media, the Boltzmann equation in the relaxation-time approximation can be expressed as

$$\boldsymbol{v}_{\boldsymbol{k},\sigma} \cdot e\boldsymbol{E} \frac{\partial f_{\boldsymbol{k},\sigma}^0}{\partial \epsilon_{\boldsymbol{k},\sigma}} = -\frac{f_{\boldsymbol{k},\sigma} - f_{\boldsymbol{k},\sigma}^0}{\tau_{\boldsymbol{k},\sigma}} \tag{8}$$

in which $\boldsymbol{E}$ is the electric field, $\boldsymbol{v}_{\boldsymbol{k},\sigma}$ denotes the hole velocity, and τ represents the relaxation time. $f_{\boldsymbol{k},\sigma}^0$ and $f_{\boldsymbol{k},\sigma}$ are the equilibrium and nonequilibrium distribution functions, respectively, which are considered to be uniform in space. This assumption is quite reasonable in the absence of spin accumulation. The spin transport and domain wall MR in the presence of spin accumulation have been studied by several authors.[25–28] The effect of spin accumulation on the domain wall MR may be significant in ballistic regime[26] but it has been shown by Simanek and Rebei that in the diffusive limit the domain wall resistance is dominated by the mechanism of Ref. 10. In other words, the spin accumulation contribution to the domain wall MR is suppressed in the diffusive limit.[27] Therefore, the spin accumulation has been left out of our calculations.

In the elastic regime, the spin-dependent relaxation time, $\tau_{\boldsymbol{k},\sigma}$, can be determined by[21]

$$[\tau_{k,\sigma}]^{-1} = \frac{L_x L_z}{(2\pi)^2} \sum_{\sigma'} \int d^2\mathbf{k}' \frac{2\pi}{\hbar} |V_{\mathbf{k}',\mathbf{k}}^{\sigma',\sigma}|^2$$
$$\times [1 - \cos(\mathbf{k}',\mathbf{k})]\delta(\epsilon_{k,\sigma} - \epsilon_{k',\sigma'}), \quad (9)$$

where the elements of the scattering matrix are related to the impurity interaction and spin-orbit couplings, i.e., $V_{\mathbf{k}',\mathbf{k}}^{\sigma',\sigma} = [H_{\mathbf{k}',\mathbf{k}}^{\sigma',\sigma}]_{im} + [H_{\mathbf{k}',\mathbf{k}}^{\sigma',\sigma}]_R + [H_{\mathbf{k}',\mathbf{k}}^{\sigma',\sigma}]_D$. The matrix elements of the interaction terms as well as the explicit form of the spin-dependent relaxation times have been calculated in the Appendix. By employing the relaxation times, the evolution of the resistivity of the domain wall is carried out as follows:

$$\mathfrak{R}^{-1} = \frac{m^* e^2}{(2\pi\hbar)^2} \sum_{\sigma=\pm} \int d^2\mathbf{k}(\mathbf{v}_k \cdot \mathbf{n}_E)^2 \tau_{k,\sigma}(\theta) \frac{1}{k_{F,\sigma}} \delta(k - k_{F,\sigma})$$
$$(10)$$

in which $k_{F,\pm} = \sqrt{k_F^2 \pm \frac{2m^*\Delta}{\hbar^2}}$ and $\mathbf{n}_E = \mathbf{E}/|\mathbf{E}|$ is unit vector along the electric field, which according to Fig. 1, identifies two transport geometries CPW ($\mathbf{n}_E = \mathbf{x}$) and CIW ($\mathbf{n}_E = \mathbf{z}$). Then, the resistivity of the domain wall for CPW and CIW geometries can be calculated by

$$\mathfrak{R}_{CPW}^{-1} = \sum_{\sigma=\pm} \frac{e^2}{(2\pi)^2} \frac{(k_{F,\sigma})^2}{m^*} \int d\theta \cos^2(\theta) \tau_{k_{F,\sigma},\sigma}(\theta)$$
$$(11a)$$

and

$$\mathfrak{R}_{CIW}^{-1} = \sum_{\sigma=\pm} \frac{e^2}{(2\pi)^2} \frac{(k_{F,\sigma})^2}{m^*} \int d\theta \sin^2(\theta) \tau_{k_{F,\sigma},\sigma}(\theta). \quad (11b)$$

If we replace the domain wall with a ferromagnet, the eigenstates of the $H_0 + H_{ex}$ will be pure spin states given by

$$|\Phi_{\mathbf{k}}^{\uparrow}\rangle = \frac{1}{\sqrt{L_x L_z}} e^{i(k_x x + k_z z)} \begin{pmatrix} 1 \\ 0 \end{pmatrix} \quad (12a)$$

and

$$|\Phi_{\mathbf{k}}^{\downarrow}\rangle = \frac{1}{\sqrt{L_x L_z}} e^{i(k_x x + k_z z)} \begin{pmatrix} 0 \\ 1 \end{pmatrix}. \quad (12b)$$

The spin-orbit interactions cannot contribute to the elastic scatterings inside a ferromagnet. Thus, only the impurity scattering as the relaxation mechanism should be taken into account for the ferromagnetic region. Since this relaxation cannot produce any spin-flip transition between the pure spin eigenstates introduced in Eq. (12), the scattering matrix of impurities inside a ferromagnet and in the spin space can be expressed as

$$[H_{\mathbf{k}',\mathbf{k}}^{\sigma',\sigma}]_{im} = \sum_j e^{i(\mathbf{k}-\mathbf{k}')\cdot\mathbf{r}_j} \begin{pmatrix} v_{im} - \Delta_{im} & 0 \\ 0 & v_{im} + \Delta_{im} \end{pmatrix}. \quad (13)$$

Similarly, for a ferromagnet, one can exhibit that the relaxation time associated with impurity scatterings is derived by the following equation:
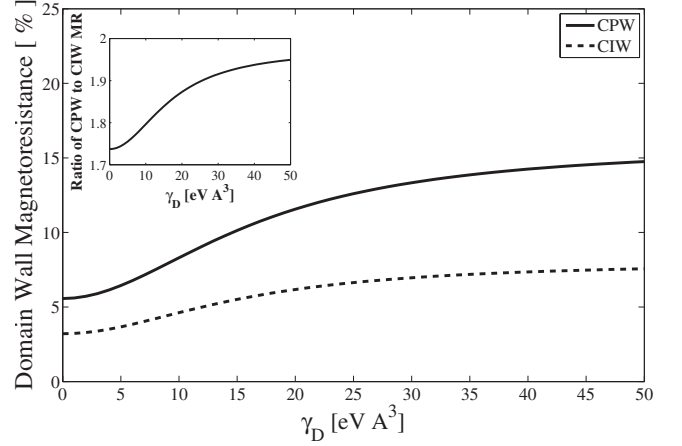
FIG. 2. The domain wall MR versus the Dresselhaus interaction strength in CPW and CIW geometries for $c_i = 1.0 \times 10^4$ cm^{-2}, $d = 15$ nm, and $p = 3.5 \times 10^{20}$ cm^{-3}. Inset: the ratio of CPW to CIW domain wall MR.

$$[\tau_\sigma]_{Ferro}^{-1} = \frac{L_x L_z m^* N_{im}(v_{im} - \sigma\Delta_{im})^2}{\hbar^3}. \quad (14)$$

As a result, the resistivity of the ferromagnet is found out to be

$$\mathfrak{R}_{Ferro} = \left[\frac{e^2}{4\pi m}(\tau_\uparrow \cdot k_{F,\uparrow}^2 + \tau_\downarrow \cdot k_{F,\downarrow}^2) \right]^{-1}. \quad (15)$$

Finally, the magnetoresistance in CPW and CIW geometries is given by

$$MR_{CPW} = \frac{\mathfrak{R}_{CPW}}{\mathfrak{R}_{Ferro}} - 1 \quad (16a)$$

and

$$MR_{CIW} = \frac{\mathfrak{R}_{CIW}}{\mathfrak{R}_{Ferro}} - 1. \quad (16b)$$

III. RESULTS AND DISCUSSION

The study on the domain wall resistance has been done for 10 nm thick diluted ferromagnetic semiconductor thin films with the parameters $\Delta = 30$ meV and $m^* = (m_{lh}^{3/2} + m_{hh}^{3/2})^{2/3} m_e = 0.47 m_e$, where m_e is the electron mass. These parameters correspond to Ga$_{0.947}$Mn$_{0.053}$As epilayers with large magnitude of critical temperature $T_C = 110$ K.[29] The density of charge carriers, the electrical potential of the localized impurities and the exchange splitting constant between holes and localized impurities have been considered to be $p = 3.5 \times 10^{20}$ cm^{-3}, $v_{im} = 1.0$ eV, and $\Delta_{im} = 0.8\Delta$, respectively. Typical domain wall width in the Bulk Mn-doped GaAs is about $d = 15$ nm.[30] The magnitude of the Fermi wavevector in such a heavily Mn-doped GaAs, can be obtained as $k_F = 2.18$ nm^{-1}. In this case, the semiclassical approximation requirement, $k_{F(\uparrow\downarrow)} d \gg 1$, is satisfied adequately.

The domain wall MR versus the Dresselhaus interaction strength is depicted in Fig. 2 for both CPW and CIW geom-
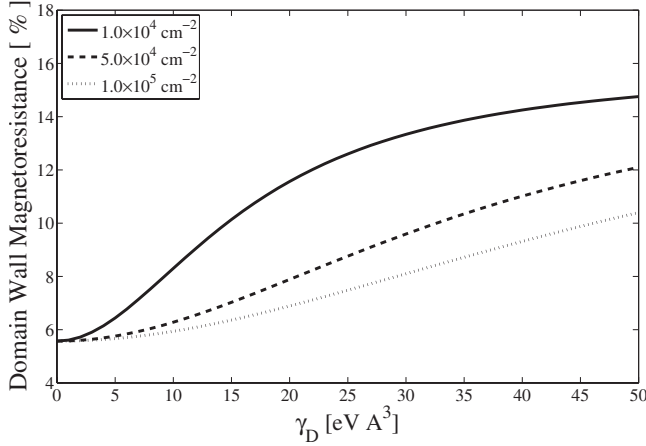
FIG. 3. The CPW domain wall MR as a function of the Dresselhaus coupling strength for different impurity concentrations, d =15 nm and $p=3.5\times10^{20}$ cm^{-3}.

FIG. 4. The CPW domain wall MR versus domain wall width for $p=3.5\times10^{20}$ cm^{-3} and $c_i=1.0\times10^{4}$ cm^{-2}. Inset: the Dresselhaus magnetic field strength experienced by holes in up to down ($\downarrow\uparrow$) and down to up ($\uparrow\downarrow$) spin-flip transitions.

etries. As can be seen, the domain wall MR in both configurations increases monotonically and then saturates at large Dresselhaus coupling strengths. As the effective magnetic field associated with the Dresselhaus spin-orbit interaction increases, the relaxation time decreases rapidly just for the four incident wavevector angles mentioned in the Appendix whereas because of impurity scattering, it remains unchanged for other incident angles. So, the domain wall MR which is calculated by integrating the relaxation times over incident wavevector angles [Eq. (11)], remains approximately constant at large Dresselhaus coupling strengths.

The inset of Fig. 2 shows the ratio of CPW to CIW magnetoresistance. The resistivity in CPW geometry is greater than that of CIW. It becomes nearly two times larger at high values of spin-orbit interaction strength which is in good quantitative agreement with the experimental reports.[31] This can be understood from the fact that the hole traveling across the domain wall in the CPW configuration encounters an effective magnetic potential barrier while in the CIW geometry, the hole adapts its magnetic moment to the local magnetization (which is homogeneous along the z direction). Therefore, carrier transport in CIW configuration is close to the adiabatic regime.

Figure 3 shows the sensitivity of the domain wall MR to the impurity density in presence of the Dresselhaus interaction. It can be realized that high impurity densities suppress the effect of the Dresselhaus interaction contribution to the CPW resistivity. The Dresselhaus interaction is more effective for low impurity concentrations. Similar results can also be found for CIW geometry. Figure 3 also demonstrates that in the absence of spin-orbit interaction, the domain wall MR does not depend on impurity density. Using Eqs. (A6) and (14), it is easy to show that $[\tau_\sigma(\theta)]_{DW}^{-1}\propto c_{im}$ and $[\tau_\sigma]_{Ferro}^{-1}\propto c_{im}$. Therefore, the dependency of the domain wall MR on the impurity density is removed from Eq. (16). The linear dependence of resistivity on c_{im} comes from the semiclassical approach in which some quantum interference effects have been discarded.

In determining the dependency of domain wall MR on given parameters, clearly, the size of the domain wall plays
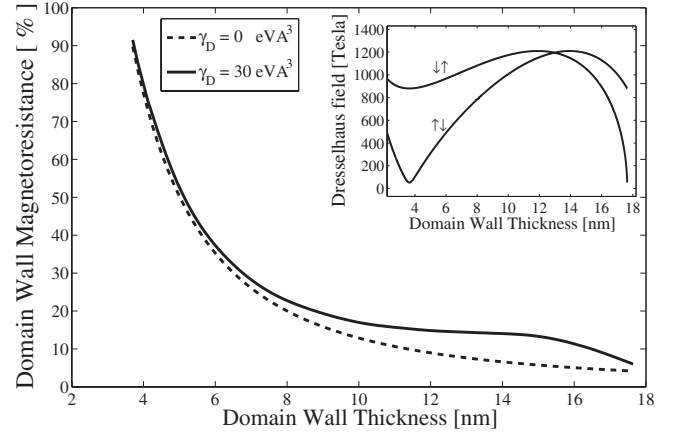
an important role. In the absence of Dresselhaus spin-orbit interaction, we expect a monotonic reduction in domain wall MR by increasing the domain wall width, as shown in Fig. 4. This is because of being close to the adiabatic limit by raising the size of the domain wall. Nevertheless, the adiabaticity can be violated by Dresselhaus spin-orbit interaction. As mentioned in the Appendix, the spin-flip scattering angles depend strongly on the domain wall width [Eqs. (A4) and (A5)]. Consequently, the effective magnetic field of the Dresselhaus spin-orbit interaction is modified by the size of the domain wall. This effective field sensed by the holes in both $\downarrow\uparrow$ and $\uparrow\downarrow$ spin-flip transitions has been shown in the inset of Fig. 4 for different domain wall widths. According to this figure, high magnetic field produced by the Dresselhaus spin-orbit interaction preserves the nonadiabatic character of the transport. This can be deduced from the plateau occurred in the domain wall MR in the presence of the Dresselhaus interaction (Fig. 4). For domain walls thicker than about 15 nm, the Dresselhaus spin-orbit effective field begins to diminish. Because of fast falling down of the effective field, the MR curve exhibits a clear change in slope around this thickness and then adiabatic transport takes place at higher thicknesses.

The domain wall width is also an important parameter in determining the contribution of different scattering mechanisms to the domain wall MR. To be more specific, we consider the Dresselhaus and the Rashba spin-orbit interactions whose effective magnetic fields have been depicted in Fig. 5. Using Eq. (A4) it is easy to show that for a 15 nm thick domain wall and a Fermi energy of 0.38 eV, the spin-orbit scatterings occur just at incident wavevector angels of 30.3°, 149.7°, 210.3°, and 329.7° for $\downarrow\uparrow$ spin-flip transitions and 39.9°, 140.1°, 219.9°, and 320.1° for $\uparrow\downarrow$ transitions. According to Fig. 5, for such a domain wall, the Dresselhaus effective magnetic field for both $\downarrow\uparrow$ and $\uparrow\downarrow$ spin-flip transitions is approximately one order of magnitude greater than that of the Rashba term. As a result, it is expected that the Dresselhaus interaction will lead to a larger spin-flip scattering and consequently to a higher domain wall MR relative to the Rashba spin-orbit interaction. This can be confirmed by Fig.
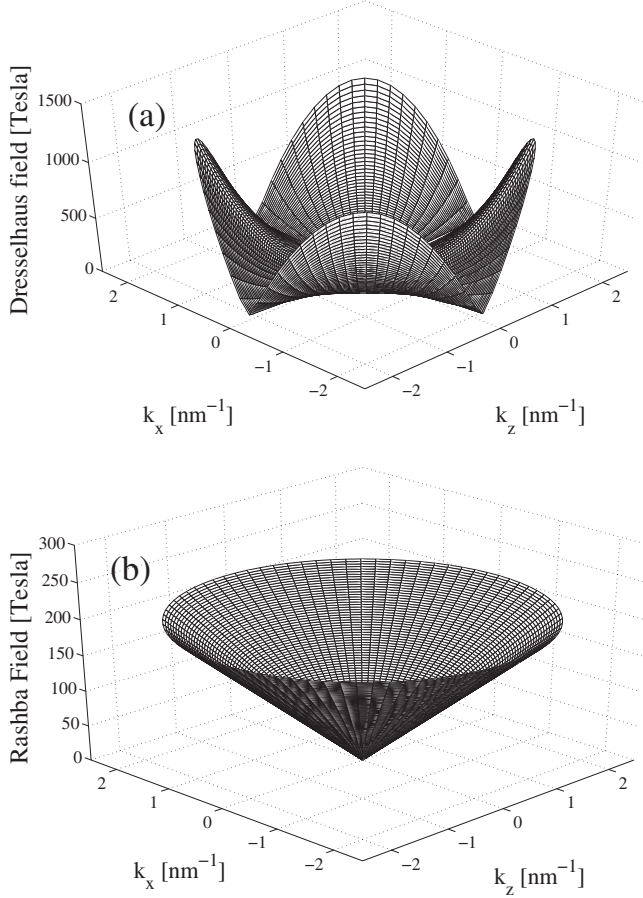
FIG. 5. The effective magnetic fields resulted from (a) the Dresselhaus and (b) the Rashba interactions as functions of in-plane wavevector of holes (k_x, k_z) for $\gamma_D = 30$ eV A^3 and $\gamma_R = 10^{-2}$ eV nm.

6 in which the domain wall MR versus the strengths of the Dresselhaus and the Rashba spin-orbit interactions is plotted as a contour graph. The strengths of the Dresselhaus and the Rashba spin-orbit couplings for a typical magnetic semiconductor are 30 eV A^3 and 10^{-2} eV nm, respectively.[32] Ac-
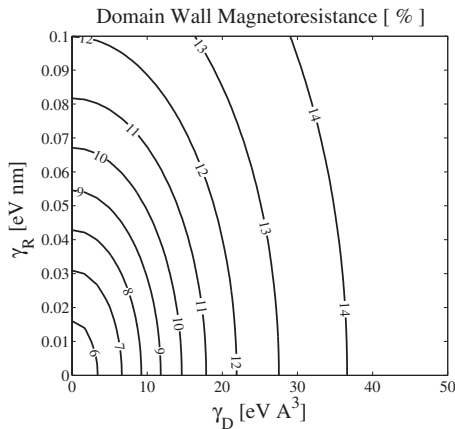
FIG. 6. Domain wall magnetoresistance as a function of both the Dresselhaus (γ_D) and the Rashba (γ_R) spin-orbit coupling strengths in CPW geometry for $d = 15$ nm, $c_i = 1.0 \times 10^4$ cm^{-2}, and $p = 3.5 \times 10^{20}$ cm^{-3}.

cordingly, it is clearly seen that the Dresselhaus term (the MR is about 13.4%) is more effective than the Rashba coupling (the MR is around 5.8%) in producing resistance. This is also the case of thicker domain walls. For instance, it is easy to show that $B_{D,\downarrow\uparrow}$ tends to diminish at a thickness around 17.7 nm and so $B_{D,\downarrow\downarrow} \ll B_R$. Nevertheless, $B_{D,\uparrow\downarrow}$ remains remarkably greater than B_R and makes the Dresselhaus coupling more effective. In such a ferromagnetic semiconductor, just for very long or very short domain walls the effects of these two spin-orbit couplings become close to each other. In the case of long domain walls, the holes follow the local magnetic moments adiabatically and for very short domain walls, the impurity relaxation mechanism suppresses the influence of spin-orbit couplings.

IV. CONCLUSION

In this study, we have investigated the influence of the Dresselhaus spin-orbit interaction on the MR of a linear smooth domain wall in a diffusive 2DEG. It has been found that the domain wall MR increases with the strength of the Dresselhaus coupling in both CPW and CIW geometries. The results show that the domain wall MR in the CPW geometry is greater than that in the CIW geometry. It has also been demonstrated that increasing impurity concentration suppresses the influence of the Dresselhaus interaction. The domain wall MR decreases monotonously as the domain wall width increases but in the presence of the Dresselhaus spin-orbit interaction, it exhibits a plateau behavior in a range of the domain wall widths. It has also been realized that for a typical magnetic semiconductor the Dresselhaus spin-orbit term can be more effective in producing resistance in comparison with the Rashba spin-orbit interaction.

APPENDIX

The matrix elements of interaction terms can be evaluated as follows:

$$[H^{\sigma',\sigma}_{\boldsymbol{k}',\boldsymbol{k}}]_{im} = \alpha(k_x)\alpha(k'_x)(v_{im} + \Delta_{im})$$
$$\times \begin{pmatrix} \Lambda + \zeta_k\zeta_{k'} & i\Lambda\zeta_k - i\zeta_{k'} \\ i\zeta_k - i\Lambda\zeta_{k'} & 1 + \Lambda\zeta_k\zeta_{k'} \end{pmatrix} \sum_j e^{i(\boldsymbol{k}-\boldsymbol{k}')\cdot\boldsymbol{r}_j},$$

$$(A1a)$$

$$[H^{\sigma',\sigma}_{\boldsymbol{k}',\boldsymbol{k}}]_R = \gamma_R\left\{\left(\frac{i\pi}{2d} - k_z\right)\Xi_1 + k_x\Xi_2\right\}, \qquad (A1b)$$

$$[H^{\sigma',\sigma}_{\boldsymbol{k}',\boldsymbol{k}}]_D = -\gamma_D\left\{\left(-\frac{\pi^2}{L_y^2}k_x - ik_xk_z\frac{\pi}{d} + k_xk_z^2\right)\Xi_1 \right.$$
$$\left. + \left(\frac{\pi^2}{L_y^2}k_z + \frac{i\pi^3}{2dL_y^2} - k_x^2k_z - \frac{\pi^2}{4d^2}k_z - \frac{i\pi}{2d}k_z^2\right)\Xi_2\right\}$$

$$(A1c)$$

in which $\Lambda = (v_{im} - \Delta_{im})/(v_{im} + \Delta_{im})$,

$$\Xi_1 = \frac{\alpha(k_x)\alpha(k_x')}{2}\{\langle\sigma'|\sigma_x - i\sigma_z|\sigma\rangle\delta_{k_x',k_x+(\pi/d)}$$
$$+ \langle\sigma'|\sigma_x + i\sigma_z|\sigma\rangle\delta_{k_x',k_x-(\pi/d)}\}\delta_{k_z',k_z}, \quad \text{(A2a)}$$

and

$$\Xi_2 = \frac{\alpha(k_x)\alpha(k_x')}{2}\{\langle\sigma'|\sigma_z + i\sigma_x|\sigma\rangle\delta_{k_x',k_x+(\pi/d)}$$
$$+ \langle\sigma'|\sigma_z - i\sigma_x|\sigma\rangle\delta_{k_x',k_x-(\pi/d)}\}\delta_{k_z',k_z}. \quad \text{(A2b)}$$

According to Fig. 1, the system under study has been confined in y direction. This confinement results in discrete transverse modes. The momentum transfer that can be obtained by a carrier due to the mentioned relaxations is much smaller than the required one for a transition between the nearest transverse modes. Thus, one can use the single-transverse mode approximation. In other words, the transport occurs mainly in two-dimensional xz plane. Within this approximation the integration in Eq. (9) has been carried out over the two-dimensional $\boldsymbol{k}$ space.

The Dirac delta functions in Eq. (9) can be written as follows:

$$\delta(\epsilon_{k,\uparrow} - \epsilon_{k',\uparrow}) = \frac{m^*}{\hbar^2 k}[\delta(k'-k) + \delta(k'+k)], \quad \text{(A3a)}$$

$$\delta(\epsilon_{k,\uparrow} - \epsilon_{k',\downarrow}) = \frac{m^*}{\hbar^2 k_-}[\delta(k'-k_-) + \delta(k'+k_-)], \quad \text{(A3b)}$$

$$\delta(\epsilon_{k,\downarrow} - \epsilon_{k',\uparrow}) = \frac{m^*}{\hbar^2 k_+}[\delta(k'-k_+) + \delta(k'+k_+)], \quad \text{(A3c)}$$

$$\delta(\epsilon_{k,\downarrow} - \epsilon_{k',\downarrow}) = \frac{m^*}{\hbar^2 k}[\delta(k'-k) + \delta(k'+k)] \quad \text{(A3d)}$$

in which $k_\pm = \sqrt{k^2 \pm \frac{4m^*\Delta}{\hbar^2}}$. The last term in each of the above equations is equal to zero because $k=|\vec{k}|$ and $k'=|\vec{k}'|$ are positive parameters. Since, $\delta(k'-k)$ and $\delta_{k_x',k_x\pm(\pi/d)}$ cannot be satisfied simultaneously, regarding Eq. (A3), we can conclude that the diagonal matrix elements of the spin-orbit interactions are zero. In addition, the nondiagonal scattering matrix elements are nonzero only for incident wavevector angles of $\theta_1 = \theta$, $\theta_2 = \pi - \theta$, $\theta_3 = \pi + \theta$, and $\theta_4 = 2\pi - \theta$ and corresponding scattering wavevector angles of $\theta_1' = \theta'$, $\theta_2' = \pi - \theta'$, $\theta_3' = \pi + \theta'$, and $\theta_4' = 2\pi - \theta'$, (see Fig. 7), where

$$\theta = \cos^{-1}\left(\pm\frac{k^2 - k_\mp^2 + \dfrac{\pi^2}{d^2}}{\dfrac{2\pi}{d}k}\right) \quad \text{(A4)}$$

and
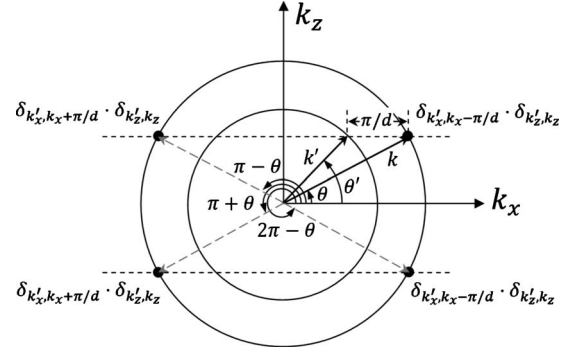
FIG. 7. View of the 2D wavevector space (k_x, k_z). The represented wavevectors satisfy functions $\delta(k'-k_-)$ and $\delta_{k_x',k_x\pm\pi/d}$, simultaneously. A similar figure can be drawn for the case of $\delta(k'-k_+)$ condition.

$$\theta' = \tan^{-1}\left(\frac{k\sin(\theta)}{k\cos(\theta) \mp \dfrac{\pi}{d}}\right). \quad \text{(A5)}$$

In these definitions, the upper and lower signs are applied to the $V_{k',k}^{\downarrow,\uparrow}$ and $V_{k',k}^{\uparrow,\downarrow}$ elements, respectively. As a consequence since the spin-orbit relaxations contribute just at the represented incident wavevector angles, the relaxation times become dependent on the incident angle.

Random distribution of the impurities results in decoupling of impurity and the spin-orbit interactions as $|V_{k',k}^{\sigma',\sigma}|^2 = |H_{k',k}^{\sigma',\sigma}|_{im}^2 + |H_{k',k}^{\sigma',\sigma}|_{spin-orbit}^2$. So, we can rewrite Eq. (9) as

$$[\tau_{k,\sigma}(\theta)]^{-1} = [\tau_{k,\sigma}(\theta)]_{im}^{-1} + [\tau_{k,\sigma}(\theta)]_{spin-orbit}^{-1} \quad \text{(A6)}$$

in which,

$$[\tau_{k,\uparrow}(\theta)]_{im}^{-1} = \frac{(L_x L_z)^2}{2\pi}\frac{m^*}{\hbar^3}c_{im}(v_{im}+\Delta_{im})^2\frac{1}{\sqrt{1+k^2\zeta^2\cos^2(\theta)}}$$
$$\times \int_0^{2\pi}d\theta'[1 - \cos(\theta-\theta')]$$
$$\times \left[\frac{|\Lambda + k^2\zeta^2\cos(\theta)\cos(\theta')|^2}{\sqrt{1+k^2\zeta^2\cos^2(\theta')}}\right.$$
$$\left.+ \frac{|ik\zeta\cos(\theta) - i\Lambda k_-\zeta\cos(\theta')|^2}{\sqrt{1+k_-^2\zeta^2\cos^2(\theta')}}\right],$$

$$[\tau_{k,\downarrow}(\theta)]_{im}^{-1} = \frac{(L_x L_z)^2}{2\pi}\frac{m^*}{\hbar^3}c_{im}(v_{im}+\Delta_{im})^2\frac{1}{\sqrt{1+k^2\zeta^2\cos^2(\theta)}}$$
$$\times \int_0^{2\pi}d\theta'[1 - \cos(\theta-\theta')]$$
$$\times \left[\frac{|1 + \Lambda k^2\zeta^2\cos(\theta)\cos(\theta')|^2}{\sqrt{1+k^2\zeta^2\cos^2(\theta')}}\right.$$
$$\left.+ \frac{|i\Lambda k\zeta\cos(\theta) - ik_+\zeta\cos(\theta')|^2}{\sqrt{1+k_+^2\zeta^2\cos^2(\theta')}}\right],$$

$$[\tau_{k,\uparrow}(\theta)]^{-1}_{spin\text{-}orbit} = \frac{L_x L_z}{4\pi} \frac{m^*}{\hbar^3} C_- \Bigg| (A+iB)D^-_{k_-} \sum_{j=2,3} \delta(\theta-\theta_j)$$

$$\times \delta(\theta'-\theta'_j) + (A-iB)D^+_{k_-}\sum_{j=1,4}$$

$$\times \delta(\theta-\theta_j)\delta(\theta'-\theta'_j)\Bigg|^2,$$

$$[\tau_{k,\downarrow}(\theta)]^{-1}_{spin\text{-}orbit} = \frac{L_x L_z}{4\pi} \frac{m^*}{\hbar^3} C_+ \Bigg| (A+iB)D^+_{k_+} \sum_{j=2,3} \delta(\theta-\theta_j)$$

$$\times \delta(\theta'-\theta'_j) + (A-iB)D^-_{k_+}\sum_{j=1,4}$$

$$\times \delta(\theta-\theta_j)\delta(\theta'-\theta'_j)\Bigg|^2,$$

where,

$$A = \gamma_R\left[\frac{i\pi}{2d} - k\sin(\theta)\right] - \gamma_D\left[-\frac{\pi^2 k}{L_y^2}\cos(\theta) - \frac{i\pi k^2}{2d}\sin(2\theta)\right.$$

$$\left. + k^3\sin^2(\theta)\cos(\theta)\right],$$

$$B = \gamma_R[k\cos(\theta)] - \gamma_D\left[\frac{\pi^2 k}{L_y^2}\sin(\theta) + \frac{i\pi^3}{2dL_y^2} - k^3\sin(\theta)\cos^2(\theta)\right.$$

$$\left. - \frac{\pi^2 k}{4d^2}\sin(\theta) - \frac{i\pi k^2}{2d}\sin^2(\theta)\right],$$

$$C_\pm = \frac{1 - \cos(\theta - \theta')}{\sqrt{1 + k^2\zeta^2\cos^2(\theta)}\sqrt{1 + k_\pm^2\zeta^2\cos^2(\theta')}},$$

$$D^\pm_{k_\pm} = [k\zeta\cos(\theta) \pm 1][k_\pm\zeta\cos(\theta') \pm 1],$$

and $c_{im} = N_{im}/(L_x \cdot L_z)$ is the density of impurity atoms.

*m-ghanaat@cc.sbu.ac.ir

[1] W. Black and B. Das, J. Appl. Phys. **87**, 6674 (2000).

[2] S. S. P. Parkin, U.S. Patent No. 6834005 (2004).

[3] J. Akerman, Science **308**, 508 (2005).

[4] I. Žutić, J. Fabian, and S. D. Sarma, Rev. Mod. Phys. **76**, 323 (2004).

[5] J. Fabian, A. Matos-Abiague, C. Ertler, P. Stano, and I. Žutić, Acta Phys. Slov. **57**, 565 (2007).

[6] T. Wosinski, T. Figielski, A. Morawski, A. Makosa, V. Osinniy, J. Wrobel, and J. Sadowski, J. Mater. Sci.: Mater. Electron. **19**, 111 (2008).

[7] C. Rüster, T. Borzenko, C. Gould, G. Schmidt, L. W. Molenkamp, X. Liu, T. J. Wojtowicz, J. K. Furdyna, Z. G. Yu, and M. E. Flatte, Phys. Rev. Lett. **91**, 216602 (2003).

[8] M. Viret, D. Vignoles, D. Cole, J. M. D. Coey, W. Allen, D. S. Daniel, and J. F. Gregg, Phys. Rev. B **53**, 8464 (1996).

[9] J. F. Gregg, W. Allen, K. Ounadjela, M. Viret, M. Hehn, S. M. Thompson, and J. M. D. Coey, Phys. Rev. Lett. **77**, 1580 (1996).

[10] P. M. Levy and S. Zhang, Phys. Rev. Lett. **79**, 5110 (1997).

[11] R. F. Sabirianov, A. K. Solanki, J. D. Burton, S. S. Jaswal, and E. Y. Tsymbal, Phys. Rev. B **72**, 054443 (2005).

[12] P. Krzysteczko and G. Dumpich, Phys. Rev. B **77**, 144422 (2008).

[13] D. Chiba, M. Yamanouchi, F. Matsukura, T. Dietl, and H. Ohno, Phys. Rev. Lett. **96**, 096602 (2006).

[14] T. Wosiński, T. Figielski, O. Pelya, A. Makosa, A. Morawski, J. Sadowski, W. Dobrowolski, R. Szymczak, and J. Wróbel, Phys. Status Solidi A **204**, 472 (2007).

[15] H. X. Tang, S. Masmanidis, R. K. Kawakami, D. D. Awschalom, and M. L. Roukes, Nature (London) **431**, 52 (2004).

[16] T. Figielski, T. Wosiński, O. Pelya, J. Sadowski, A. Morawski, A. Makosa, W. Dobrowolski, R. Szymczak, and J. Wróbel, in *Physics, Chemistry and Applications of Nanostructures*, edited by V. E. Borisenko, S. V. Gaponenko, and V. S. Gurin (World Scientific, Singapore, 2005), pp. 289–292.

[17] F. X. Bronold, I. Martin, A. Saxena, and D. L. Smith, Phys. Rev. B **66**, 233206 (2002).

[18] R. Oszwałdowski, J. A. Majewski, and T. Dietl, Phys. Rev. B **74**, 153310 (2006).

[19] A. K. Nguyen, R. V. Shchelushkin, and A. Brataas, Phys. Rev. Lett. **97**, 136603 (2006).

[20] V. K. Dugaev, J. Barnaś, J. Berakdar, V. I. Ivanov, W. Dobrowolski, and V. F. Mitin, Phys. Rev. B **71**, 024430 (2005).

[21] A. Phirouznia, M. M. Tehranchi, and M. Ghanaatshoar, Phys. Rev. B **75**, 224403 (2007).

[22] M. Ghanaatshoar, V. Fallahi, M. M. Tehranchi, and A. Phirouznia, IEEE Trans. Magn. **44**, 3127 (2008).

[23] G. Tatara and H. Fukuyama, Phys. Rev. Lett. **78**, 3773 (1997).

[24] V. K. Dugaev, J. Barnaś, A. Lusakowski, and L. A. Turski, J. Supercond. Novel Magn. **16**, 15 (2003).

[25] E. Šimánek, Phys. Rev. B **63**, 224412 (2001).

[26] M. Dzero, L. P. Gorkov, A. K. Zvezdin, and K. A. Zvezdin, Phys. Rev. B **67**, 100402 (2003).

[27] E. Šimánek and A. Rebei, Phys. Rev. B **71**, 172405 (2005).

[28] T. Taniguchi, J. Sato, and H. Imamura, Phys. Rev. B **79**, 212410 (2009).

[29] T. Dietl, H. Ohno, and F. Matsukura, Phys. Rev. B **63**, 195205 (2001).

[30] T. Dietl, J. Konig, and A. H. MacDonald, Phys. Rev. B **64**, 241201 (2001).

[31] T. Manago, A. Sinsarp, and H. Akinaga, J. Appl. Phys. **102**, 033920 (2007).

[32] R. Winkler, *Spin-Orbit Coupling Effects in Two-Dimensional Electron and Hole Systems*, Springer Tracts in Modern Physics (Springer, Berlin/Heidelberg, 2003).